European Journal of Medicinal Chemistry 203 (2020) 112576

Contents lists available at ScienceDirect

European Journal of Medicinal Chemistry

journal homepage: http://www.elsevier.com/locate/ejmech

# Mechanisms underlying the cytotoxic activity of syn/anti-isomers of dinuclear Au(I) NHC complexes

Bruno Dominelli [a, 1], Christian H.G. Jakob [a, 1], Jens Oberkofler [a], Pauline J. Fischer [a], Eva-Maria Esslinger [a], Robert M. Reich [a], Fernanda Marques [b], Teresa Pinheiro [c], João D.G. Correia [b], Fritz E. Kühn [a, *]

[a] Faculty of Chemistry and Catalysis Research Center, Molecular Catalysis, Technische Universität München, Lichtenbergstr. 4, D-85748, Garching bei München, Germany
[b] Centro de Ciências e Tecnologias Nucleares and Departamento de Engenharia e Ciências Nucleares, Instituto Superior Técnico, Universidade de Lisboa, Campus Tecnológico e Nuclear, Estrada Nacional Nº 10 (km 139,7), 2695-066, Bobadela, LRS, Portugal
[c] IBB-Institute for Bioengineering and Biosciences and Departamento de Engenharia e Ciências Nucleares, Instituto Superior Técnico, Universidade de Lisboa, Av. Rovisco Pais 1, 1049-001, Lisboa, Portugal

ARTICLE INFO

*Article history:*
Received 19 May 2020
Received in revised form
10 June 2020
Accepted 11 June 2020
Available online 16 July 2020

*Keywords:*
Dinuclear gold(I) complexes
Bridge-functionalized NHC
Syn and anti-isomers
Counter-anion exchange
Antiproliferative activity
TrxR inhibition

ABSTRACT

The syn- and anti-isomers of dinuclear Au(I) complexes of the type $\mathbf{Au_2(^{R}L^{OH})(PF_6)_2}$ (R = isopropyl or mesityl) bearing 2-hydroxyethane-1,1-diyl-bridged bisimidazolylidene ligands were separated by reversed phase high performance liquid chromatography (HPLC) and characterized by NMR spectroscopy, elemental analysis, ESI mass spectrometry as well as single crystal X-ray diffraction analysis. Evaluation of the antiproliferative activity of the isolated isomers has shown very small difference in their cytotoxic behavior in various cancer cell lines. Additional counter-anion exchange (hexafluorophosphate to chloride) allows to increase the water solubility of $\mathbf{^{syn}Au_2(^{Mes}L^{OH})(PF_6)_2}$ and leads to higher antiproliferative activity when compared to the hexafluorophosphate-complex. Both isomers were treated with L-cysteine as nucleophilic thiol source and only the anti-isomer shows dissociation of one bisimidazolylidene ligand after 24 h. In the case of the syn-isomer, density functional theory calculations indicate a lower reactivity due to the higher steric hindrance of the *N*-substituents and additional hydrogen bond interaction, which prevents a nucleophilic attack. When the *N*-substituent is replaced by the bulkier mesityl group, both conformations remain unreactive and result to be the most cytotoxic complexes in the above-mentioned cancer cell lines. Interestingly, $\mathbf{^{syn}Au_2(^{Mes}L^{OH})(PF_6)_2}$ exhibits a high selectivity in the MCF-7 cell line with a selectivity index (SI) of 19, which is superior to auranofin (SI < 1), making this compound an ideal candidate for further studies. Preliminary mechanistic studies reveal that the cytotoxic complexes possess mitochondrial-TrxR inhibition properties in the nanomolar range. Additionally, the cellular distribution studies by ICP-MS and nuclear microscopy have shown that the compound accumulates in the membranes. These results suggest that the mitochondrial membrane is the main target for this type of dinuclear complexes, causing oxidative stress by inhibiting mitochondrial thioredoxin reductase.



## 1. Introduction

In recent years, interest in the application of gold(I) organometallic complexes as potential anticancer agents increased notably [1–5]. Indeed, gold complexes are considered as possible alternatives to platinum-based drugs (*e.g.* cisplatin and analogues) due to their more selective mode of action (Fig. 1) [6]. In this way it seems possible to overcome some of the main issues associated with current cancer chemotherapy, namely drug-resistance and low selectivity [7–10].

Auranofin, which has been tested in a Phase I and II clinical study in Chronic Lymphocytic Leukemia (CLL), is currently the most promising gold-based compound for cancer treatment (Fig. 1) [11]. Among the various types of ligands used in metal complexes for

* Corresponding author.
*E-mail address:* fritz.kuehn@ch.tum.de (F.E. Kühn).
[1] These authors contributed equally to this work.

https://doi.org/10.1016/j.ejmech.2020.112576
0223-5234/

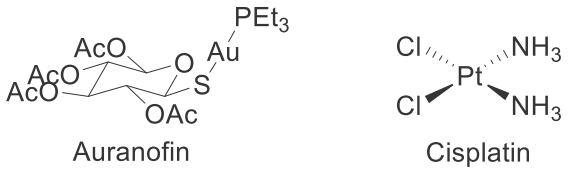


**Fig. 1.** Cisplatin and Auranofin, the clinically applied metallodrugs.

anticancer studies, *N*-heterocyclic carbene (NHC) moieties are highly versatile in their tunability allowing a hydrophilic-lipophilic balance and leading to very stable gold(I) complexes [12]. In addition, the imidazolium moieties are not cytotoxic, rendering this class of ligands more attractive when compared to the cytotoxic phosphines [3]. Gold(I) NHC complexes emerged as a new class of mitochondrial-targeting anticancer compounds after the pioneering work of Berners-Price et al. in 2004 [13]. Motivated by this report, a rising number of compounds appeared, showing promising antiproliferative activity in numerous cancer cell lines [1,2,14,15]. Especially bidentate NHC moieties allow the synthesis of extremely stable dinuclear gold(I) complexes in a metallacyclic fashion (e.g. **$Au_2(^{Me}L)_2(PF_6)_2$**, 2) and more lipophilic scaffolds have shown promising anticancer activity as well [1,2,16]. Gold NHC complexes accumulate in mitochondria due to the delocalized lipophilic cationic character (DLC), similarly to bidentate phosphine-type moieties [17,18]. In addition, the driving force for the permeability of cationic compounds in mitochondria is the mitochondrial membrane potential, being more negative in some carcinoma cells when compared to healthy cells [19]. The accepted mode of action is the inhibition of the cysteine-selenocysteine active centre of the mitochondrial or (cytosolic) enzyme thioredoxin reductases (TrxR), leading to the disruption of the enzymatic cascade reactions regulating reactive oxygen species (ROS) [20–24]. As a consequence, a programmed cell death (apoptosis) is caused by oxidative stress. Dinuclear moieties, in contrast to mononuclear complexes, possess a moderate reactivity (stability) in presence of thiol groups, thus avoiding irreversible ligand exchange reactions with thiolates present in blood (glutathione or serum albumine) [17,25]. Nevertheless, metallacyclic gold(I)-based complexes inhibit TrxR, although they are stable in the presence of thiols [26].

Besides the *N*-substituents (wingtips) and backbone positions, the modification of the bridging unit allows the access to a new functionalization pathway of multidentate NHC moieties [30]. Recently, dinuclear gold(I) complexes bearing 2-hydroxyethane-1,1-diyl- and 2,2-acetate-bridged bisimidazolylidene ligands were reported (Fig. 2), showing the formation of syn- and anti-isomer mixtures [27–29]. The formation of constitutional syn/anti-isomers was already reported for dinuclear gold(I) complexes with various bidentate ligands (e.g. diisocyano-, dithiophosphonates-, diNHC-ligands etc.) [31–41]. Combining lipophilic mesityl *N*-substituents and a more hydrophilic hydroxyethyl-bridge, the respective gold(I) complex show, however, poor water solubility and moderate cytotoxicity in HepG2 and A549 cancer cell lines [28].

Considering the previously reported formation of syn-/anti-isomers and high stability against thiols of dinuclear Au(I) NHC complexes, this work focusses on the assessment of the cytotoxic properties of the isolated isomers of **$Au_2(^{iPr}L^{OH})(PF_6)_2$** and **$Au_2(^{Mes}L^{OH})(PF_6)_2$** (Scheme 1) in different cancer cell lines, including the effect of counter-anion exchange and the stability towards L-cysteine. Aiming to an at least preliminary mechanistic insight, the ability of dinuclear Au(I) NHC complexes to inhibit isolated thioredoxin reductases, known as preferential target of Au compounds, has been examined. Moreover, cellular distribution studies by ICP-MS and nuclear microscopy are conducted to examine their putative targets.

## 2. Results and discussion

### 2.1. Separation and characterization of syn- and anti-isomers

Complexes **$^{mix}Au_2(^{iPr}L^{OH})(PF_6)_2$** and **$^{mix}Au_2(^{Mes}L^{OH})(PF_6)_2$** were synthesized as a mixture of isomers, following a transmetallation route as described in the literature (Scheme 1) [28].

The syn- and anti-isomers of **$^{mix}Au_2(^{iPr}L^{OH})(PF_6)_2$** can be separated by semi-preparative reversed phase high performance liquid chromatography (RP-HPLC) as confirmed by NMR spectroscopy (Fig. 3) and elemental analysis of the respective isolated pure isomers.

The respective resonance pattern of the two isomers can be unambiguously assigned after identifying fraction 1 (retention time (RT) = 12.65 min) as **$^{anti}Au_2(^{iPr}L^{OH})(PF_6)_2$** and fraction 2 (RT = 14.08 min) as **$^{syn}Au_2(^{iPr}L^{OH})(PF_6)_2$** by single crystal X-ray diffraction (separation details are summarized in the experimental part). Suitable crystals of **$^{syn}Au_2(^{iPr}L^{OH})(PF_6)_2$** were obtained by slow diffusion of diethyl ether into a solution of the complex in acetonitrile. A summary of the crystal data, structure solution and refinement parameters are given in the Supplementary Information (SI) (Table 2). An ORTEP-style view of the molecular structure of **$^{syn}Au_2(^{iPr}L^{OH})(PF_6)_2$**, together with selected bond lengths and angles are given in Fig. 4.

Complex **$^{syn}Au_2(^{iPr}L^{OH})(PF_6)_2$** crystallizes in the triclinic space group P1. The unit cell shows the presence of a second molecule of the same complex but with a chloride counter-ion instead of hexafluorophosphate(V) $(PF_6)^-$, **$^{syn}Au_2(^{iPr}L^{OH})(PF_6)(Cl)_2$**. An interaction between the hydroxyl groups and the co-crystallized chloride is observed. The relevant bond lengths and angles presented in Fig. 4 do not show significant differences to the previously reported anti-isomer [28]. The additional presence of chloride enhances the distance between both Au(I) nuclei of **$^{syn}Au_2(^{iPr}L^{OH})(PF_6)(Cl)_2$** to 3.76 Å when compared to **$^{syn}Au_2(^{iPr}L^{OH})(PF_6)_2$** (3.60 Å). In both cases, the distances are not in the range of aurophilic interactions [28].

The complex **$^{mix}Au_2(^{Mes}L^{OH})(PF_6)_2$**, where the *N*-substituent has been replaced by a mesityl group was synthesized similarly to **$^{mix}Au_2(^{i}PrL^{OH})(PF_6)_2$** (Scheme 1) and obtained as a mixture of isomers [28]. The attempts to separate the isomers by semi-preparative RP-HPLC resulted in the isolation of the isomer **$^{syn}Au_2(^{Mes}L^{OH})(PF_6)_2$** with high purity as ascertained by NMR spectroscopy (SI-Fig. 7). The other fraction **$^{anti,mix}Au_2(^{Mes}L^{OH})(PF_6)_2$** contains mainly the anti-isomer and as minor species other constitutional isomers (~15%, quantified *via* $^1$H NMR spectroscopy) (SI-Fig. 6) as the respective ESI-MS of the mixture showed only one mass signal (SI-Fig. 8). In accordance with previously reported DFT calculations, the functionalization of the methylene bridge deliver up to six possible isomers [28]. Thereby, the syn-and anti-exo moieties (rest riding on the methylene bridge is pointing away from the metallacycle) have been predicted to be the energetically most favored and indeed, until now the only conformations being structurally confirmed by single crystal XRD. Varying the *N*-substituents to more bulky units leads to the formation of more than two isomers in small quantities.

The moderate cytotoxic properties of the previously reported **$^{syn}Au_2(^{Mes}L^{OH})(PF_6)_2$** have been tentatively assigned to its poor water solubility [28]. Therefore, aiming to increase solubility in aqueous solutions and, consequently, improve its antiproliferative activity, **$^{syn}Au_2(^{Mes}L^{OH})(PF_6)_2$** was treated with a strong basic anion exchange resin (Amberlite IRA-400 chloride form) to replace the $(PF_6)^-$ counter-anion by chloride, yielding **$^{syn}Au_2(^{Mes}L^{OH})(Cl)_2$**

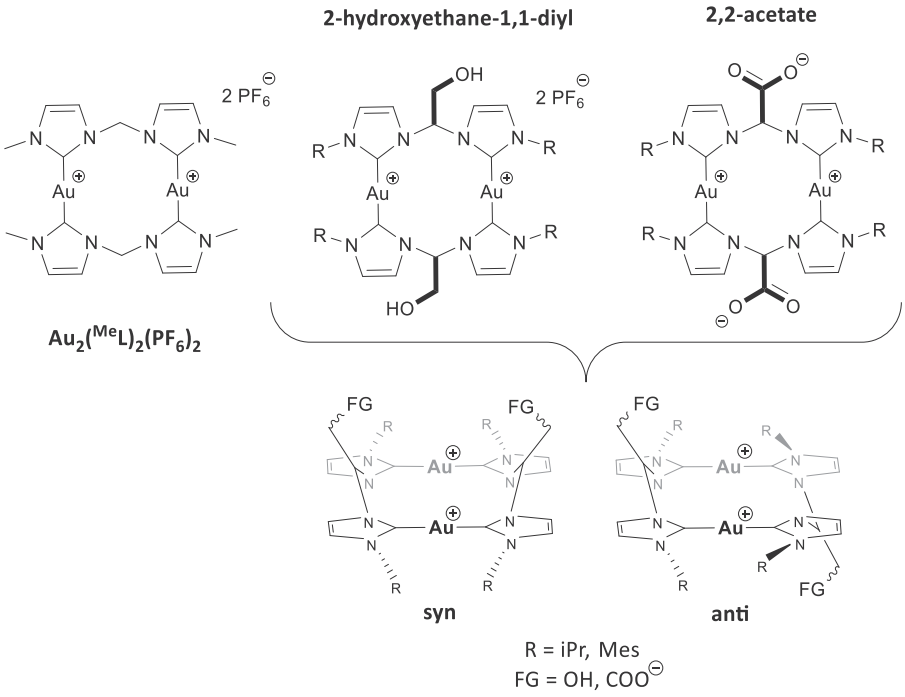


**Fig. 2.** Structure of $Au_2(^{Me}L)_2(PF_6)_2$ and general structure motifs of recently published dinuclear complexes bearing 2-hydroxyethane-1,1-diyl- or 2,2-acetate-bridged bisimidazolylidene ligands, including the visualization of the syn- and anti-isomers [27–29].

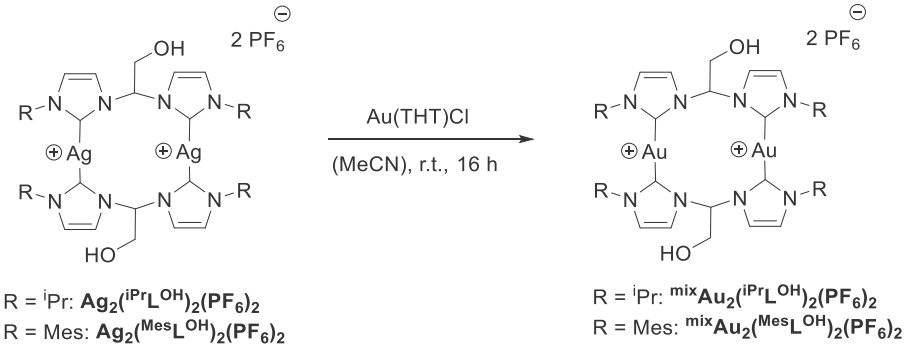


**Scheme 1.** Synthesis of $^{mix}Au_2(^{iPr}L^{OH})(PF_6)_2$ and $^{mix}Au_2(^{Mes}L^{OH})(PF_6)_2$ [28]. Abbreviations: $^{i}$Pr = isopropyl, Mes = mesityl, THT = tetrahydrothiophene.

(Scheme 2). The water solubility of $^{syn}Au_2(^{Mes}L^{OH})(Cl)_2$ is indeed significantly improved and, contrary to $^{syn}Au_2(^{Mes}L^{OH})(PF_6)_2$, a $^1$H NMR spectrum can be recorded in $D_2O$ (SI-Fig. 12). The influence of counter-anion on the solubility was already observed in literature for other anions (e.g. acetate) [42,43].

The $^{19}$F NMR spectrum (SI-Fig. 11) of $^{syn}Au_2(^{Mes}L^{OH})(Cl)_2$ reveals only traces of the $(PF_6)^-$ anion (doublet at $\delta = -81$ ppm), in relation to the reference compound (fluorobenzene, triplet of triplet at $\delta = -115$ ppm). Moreover, the elemental analysis results are in accordance with the expected theoretical values, confirming an exchange rate >99%. The $^1$H NMR spectra of $^{syn}Au_2(^{Mes}L^{OH})(PF_6)_2$ and $^{syn}Au_2(^{Mes}L^{OH})(Cl)_2$ in the same solvent ($CD_3CN$) presented different chemical shifts patterns with the exception of those of the mesityl *N*-substituents (Fig. 5).

The resonance of the hydroxyl group disappears and the $CH_2$ group (c) switches from triplet to a doublet in the spectrum of $^{syn}Au_2(^{Mes}L^{OH})(Cl_2)$. This behavior indicates an interaction between the hydroxyl group and chloride counter-anion similar to the interaction observed in the single crystal structure of $^{syn}Au_2(^{iPr}L^{OH})(PF_6)(Cl)_2$. Additionally, the OH···Cl interaction affects the proton of the bridge (a), which shows a downfield-shift.

### 2.2. Reactivity studies in the presence of L-cysteine

One of the main requirements for the use of metal complexes as potentially useful anticancer agents is high stability against nucleophilic functional groups in biological systems, namely thiol groups present in blood glutathione or in cysteine side chains of proteins. With the aim of studying the influence of the hydroxyl group and conformation on the reactivity towards thiol-containing substrates, the isomers $^{syn}Au_2(^{iPr}L^{OH})(PF_6)_2$ and $^{anti}Au_2(^{iPr}L^{OH})(PF_6)_2$ were treated with L-cysteine (4.5 eq., 37 °C) following a literature procedure [28]. Interestingly, only $^{anti}Au_2(^{iPr}L^{OH})(PF_6)_2$ reacts with L-cysteine as confirmed by ESI-MS analysis of the reaction mixture, where a single ligand exchange conversion is observed and one bisimidazolylidene ligand has been replaced by two thiolates (Fig. 6).

$^{syn}Au_2(^{iPr}L^{OH})(PF_6)_2$ is unreactive under these conditions. The

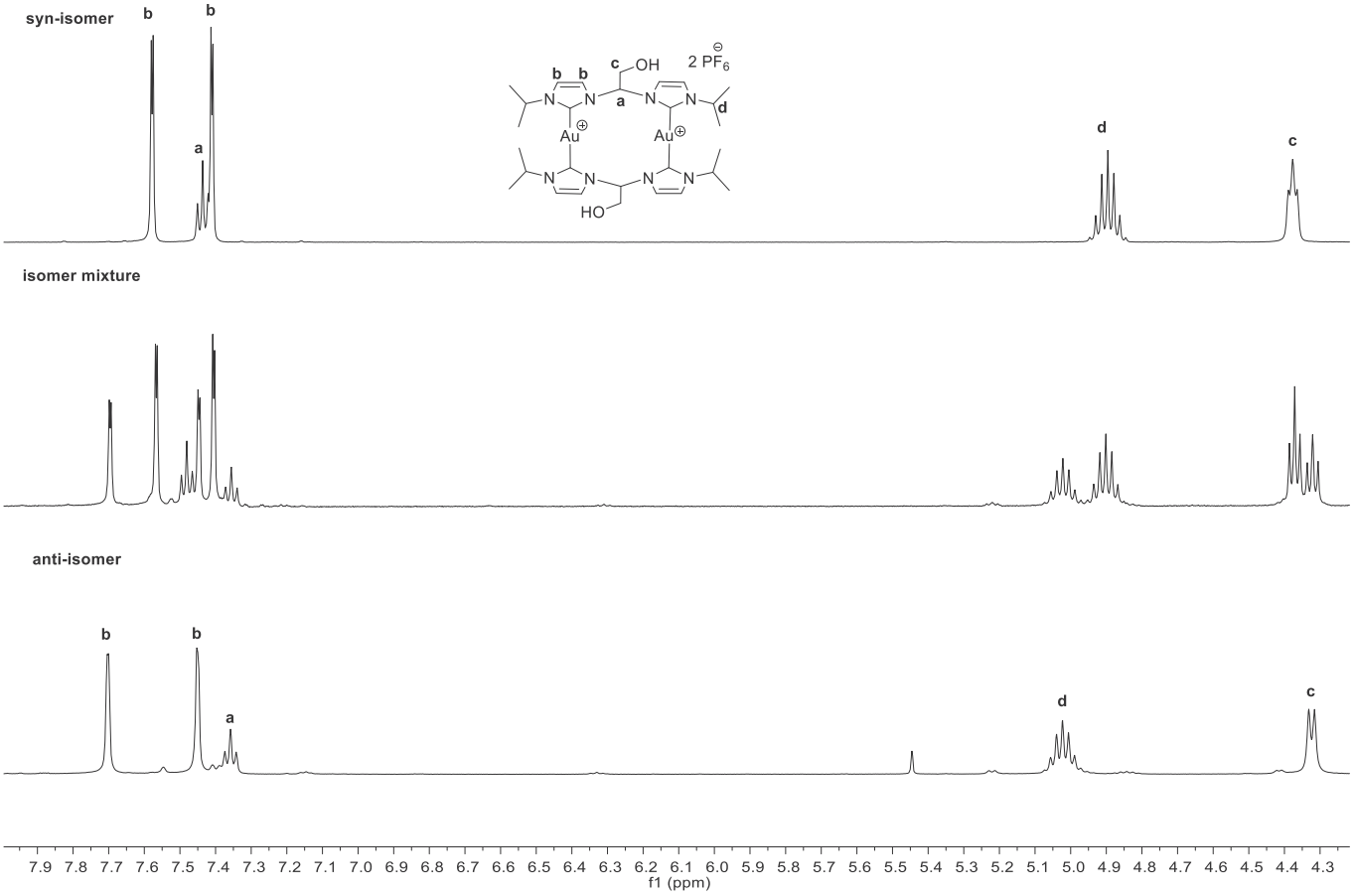


**Fig. 3.** Stacked $^{1}$H NMR spectra of $^{syn}Au_2(^{iPr}L^{OH})_2(PF_6)_2$ (top), $^{mix}Au_2(^{iPr}L^{OH})_2(PF_6)_2$ (middle) and $^{anti}Au_2(^{iPr}L^{OH})_2(PF_6)_2$ (bottom) between 8.0 ppm and 4.2 ppm in $CD_3CN$ at room temperature.

**Table 1**
Antiproliferative studies/$IC_{50}$ values of all complexes presented herein after incubation for 48 h in the human cancer cells HeLa and HepG2. Auranofin was included as a gold-reference compound.

| | HeLa | HepG2 |
|---|---|---|
| | *$IC_{50}$ [μM]* | |
| $^{anti}[Au_2(^{OH}L^{iPr})_2](PF_6)_2$ | >100 | >100 |
| $^{syn}[Au_2(^{OH}L^{iPr})_2](PF_6)_2$ | >100 | >100 |
| $^{anti,\ mix}[Au_2(^{OH}L^{Mes})_2](PF_6)_2$ | 11.3 ± 3.17 | 20.5 ± 2.31 |
| $^{syn}[Au_2(^{OH}L^{Mes})_2](PF_6)_2$ | 7.9 ± 1.9 | 13.4 ± 3.17 |
| $^{syn}[Au_2(^{OH}L^{Mes})_2]Cl_2$ | 10.3 ± 3.58 | 1.85 ± 0.05 |
| **Auranofin** | 1.23 ± 0.04 | 1.47 ± 0.02 |

higher lability of the anti-isomer in presence of nucleophiles was already observed in previously reported protonation studies of carboxylate-bridged bisimidazolylidene systems [29]. Additionally, NMR experiments are in accordance to the ESI-MS results. When repeating the same reaction with L-cysteine at an elevated temperature (50 °C), the respective NMR and ESI-MS spectra indicated the presence of the same decomposition products as described for the anti-isomer (SI-Figs. 20 and 21). Thus, the syn-isomer seems to be less accessible for thiols, since higher temperature is needed for decomposition in presence of L-cysteine. The study was also conducted with a methylene bridge-unmodified complex, $Au_2(^{Me}L)_2(PF_6)_2$ (Fig. 2), in order to analyse the influence of functional groups on the stability towards L-cysteine. The respective NMR and ESI-MS spectra (SI-Figs. 15 and 16) showed analogue decomposition products as for $^{anti}Au_2(^{iPr}L^{OH})(PF_6)_2$. However, when comparing the final $^{1}$H NMR spectra of $^{anti}Au_2(^{iPr}L^{OH})(PF_6)_2$ and $Au_2(^{Me}L)_2(PF_6)_2$ after 24 h reaction time, the residual resonances of $^{anti}Au_2(^{iPr}L^{OH})(PF_6)_2$ are remarkably smaller than those of $Au_2(^{Me}L)_2(PF_6)_2$. Thus, the presence of hydroxyl groups seems to

**Table 2**
Antiproliferative studies/$IC_{50}$ values of the complex presented herein after incubation for 48 h in human cancer cell lines and one healthy cell line (V79). Auranofin and cisplatin were included as reference compounds.

| | A2780 | A2780cisR | PC3 | MCF-7 | MDA-MB-231 | V79 |
|---|---|---|---|---|---|---|
| $IC_{50}$ [μM] | | | | | | |
| $^{syn}[Au_2(^{OH}L^{Mes})_2](PF_6)_2$ | 3.00 ± 0.6 | 2.76 ± 0.6 | 7.66 ± 3.3 | 1.22 ± 0.7 | 18.5 ± 5 | 22.9 ± 3.0 |
| **Cisplatin** | 3.6 ± 1.3 | 23 ± 2.6 | 34 ± 5.5 | 21 ± 6.3 | 13.8 ± 4.5 | 6.7 ± 2.7 |
| **Auranofin** | 0.43 ± 0.23 | 0.64 ± 0.07 | 2.4 ± 1.9 | 0.28 ± 0.14 | 1.19 ± 0.27 | 0.27 ± 0.1 |

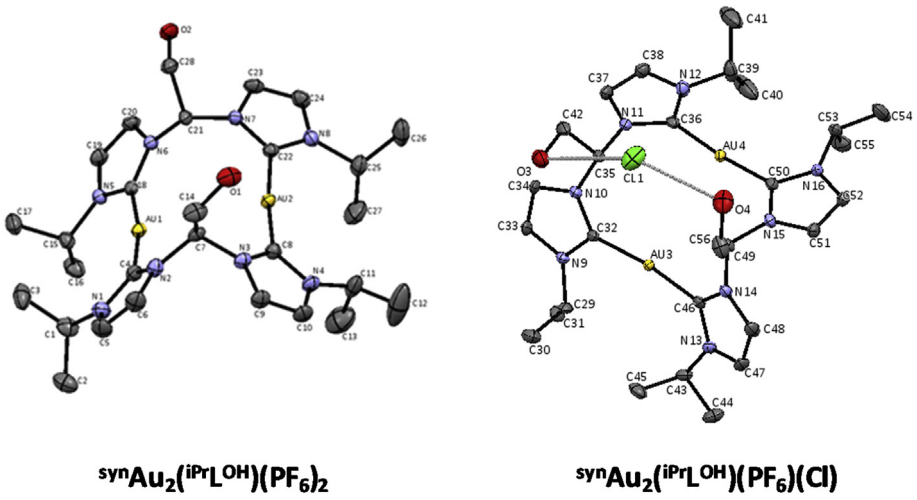


**Fig. 4.** ORTEP-style view of the cationic fragment $^{syn}$Au-$^{i}$Pr-$PF_6$ (left) and cationic fragment with co-crystallized chloride (right). All atoms are shown using ellipsoids at a probability level of 50%. Hydrogen atoms and counter-anions are omitted for clarity. Relevant bond lengths [Å] and angles [°] of $^{syn}$**Au$_2$($^{iPr}$L$^{OH}$)(PF$_6$)$_2$**: Au1–C4 2.015, Au1–C18 2.021, Au2–C8 2.022, Au2–C22 2.024, C21–N6 1.467, C21–N7 1.463, C7–N2 1.463, C7–N3 1.462; Au1···Au2 3.607; C4–Au1–C18 170.32, C8–Au2–C22 174.17, N2–C7–N3 108.63, N6–C21–N7 110.43. Relevant bond lengths [Å] and angles [°] of $^{syn}$**Au$_2$($^{iPr}$L$^{OH}$)(PF$_6$)(Cl)**: Au3–C32 2.021, Au3–C46 2.024, Au4–C36 2.026, Au4–C50 2.026, C35–N10 1.457, C35–N11 1.455, C49–N14 1.454, C49–N15 1.451; Au3···Au4 3.758; C32–Au3–C46 172.08, C36–Au4–C50 174.66, N10–C35–N11 111.13, N14–C49–N15 111.43; O3···Cl1 3.211 Å O4···Cl1 3.084 Å.

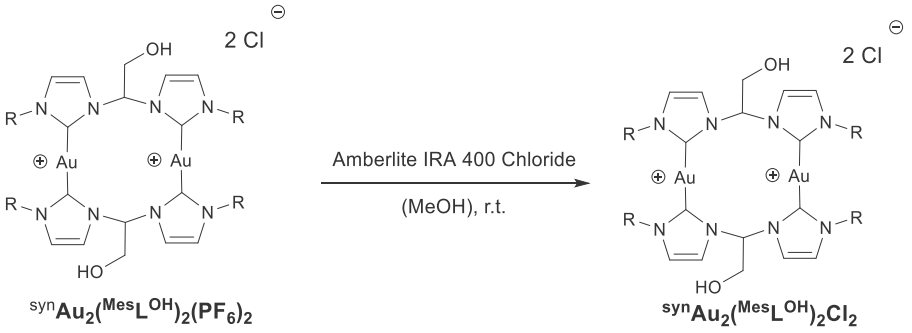


**Scheme 2.** Synthesis of $^{syn}$**Au$_2$($^{Mes}$L$^{OH}$)Cl$_2$** *via* counter-anion exchange.

improve the reactivity towards L-cysteine by facilitating the nucleophilic attack *via* hydrogen bond interactions with the carboxylic or amino group of the substrate.

The exchange of *N*-isopropyl substituents for *N*-mesityl substituents leads to improved stability of $^{anti,mix}$**Au$_2$($^{Mes}$L$^{OH}$)(PF$_6$)$_2$** and $^{syn}$**Au$_2$($^{Mes}$L$^{OH}$)(PF$_6$)$_2$** against nucleophilic attack of L-cysteine, since no changes can be observed in the respective NMR spectra (SI-Figs. 22 and 23, respectively). Sterically more hindered groups have been already reported to minimize the reactivity of Au(I)-based NHC complexes in presence of thiolates [28].

In order to understand the different reactivity of the two isomers of **Au$_2$($^{iPr}$L$^{OH}$)(PF$_6$)$_2$**, density functional theory calculations were conducted (Scheme 3). To ensure comparability to already published results, the density functional ωB97x-D as well as the basis sets 6-31 + G* and LANL2DZ (including ECP for metals; ECP: effective core potential) were employed [28].

Owing to the steric repulsion of the bulky N-substituents the $^{syn}$**Au$_2$($^{iPr}$L$^{OH}$)(PF$_6$)$_2$** is bent and the gold nuclei are shielded from one side. In the case for $^{anti}$**Au$_2$($^{iPr}$L$^{OH}$)(PF$_6$)$_2$**, the wingtips are trans positioned, allowing a nucleophilic attack from both sides. Moreover, due to the syn-rearrangement of the hydroxyl groups, two hydrogen bonds can be formed with one cysteine molecule. This prevents a nucleophilic attack, due to the fixed structure. In the case of the anti-isomer, only one hydrogen bond is formed, directing the sulphur to the gold nuclei.

### 2.3. Antiproliferative activity

The antiproliferative properties of $^{syn}$**Au$_2$($^{iPr}$L$^{OH}$)(PF$_6$)$_2$**, $^{anti}$**Au$_2$($^{iPr}$L$^{OH}$)(PF$_6$)$_2$**, $^{syn}$**Au$_2$($^{Mes}$L$^{OH}$)(X$^-$)$_2$** (X = Cl, $PF_6$), $^{anti,mix}$**Au$_2$($^{Mes}$L$^{OH}$)(PF$_6$)$_2$**, and of the reference drug auranofin were assayed by monitoring their ability to inhibit cell growth. Their cytotoxic activity was initially screened on the human cervix epitheloid carcinoma (HeLa) cell line and on the human hepatocellular carcinoma (HepG2) cell line by a colorimetric method (3-(4,5-dimethylthiazol-2-yl)-2,5-diphenyltetrazolium bromide, MTT assay). Using an appropriate range of concentrations, dose-response curves after 48 h incubation time were obtained and the corresponding $IC_{50}$ values for all compounds were calculated (Table 1).

Analysis of the results allows to conclude that the complex with *N*-isopropyl substituents **Au$_2$($^{iPr}$L$^{OH}$)(PF$_6$)$_2$** does not display any cytotoxic activity in the cancer cell lines tested, independently of the isomer used ($IC_{50}$ > 100 μM for the syn- and anti-isomer). For the complexes $^{syn}$**Au$_2$($^{Mes}$L$^{OH}$)(X$^-$)$_2$** (X = Cl, $PF_6$) and $^{anti,mix}$**Au$_2$($^{Mes}$L$^{OH}$)(PF$_6$)$_2$** a significant improvement in their cytotoxic properties is observed, with $IC_{50}$ values ranging from 1.85 ± 0.05 μM to 20.5 ± 2.31 μM. This improvement in cytotoxic

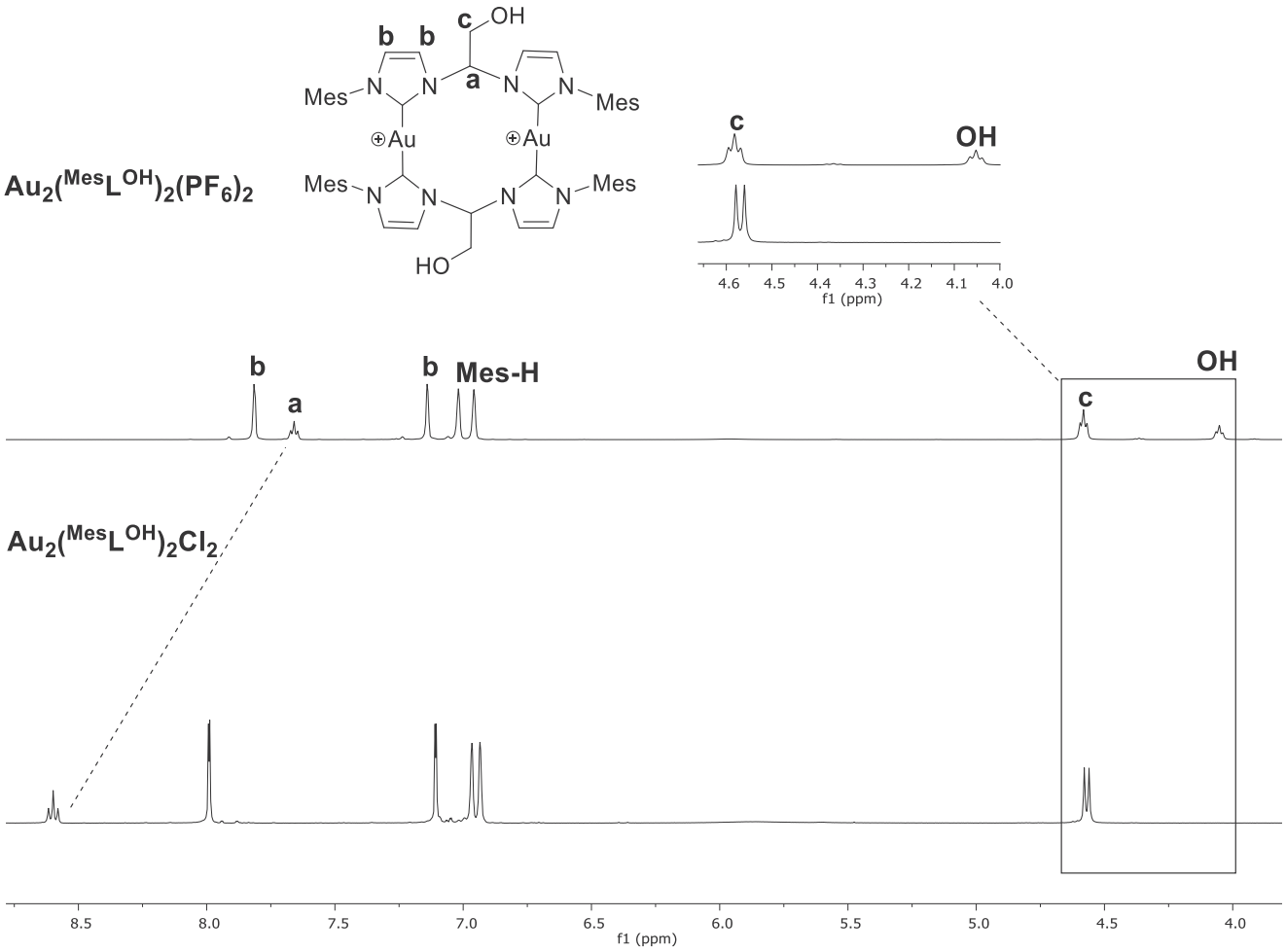


**Fig. 5.** $^{1}$H NMR spectra of $^{syn}Au_2(^{Mes}L^{OH})(PF_6)_2$ (top) and $^{syn}Au_2(^{Mes}L^{OH})(Cl)_2$ (bottom) between 8.75 ppm and 4.25 ppm in $CD_3CN$ at room temperature.

activity can be assigned to the more pronounced lipophilic character associated to the presence of the aromatic *N*-mesityl groups compared to isopropyl. This trend is in accord with the observed trends reported in literature, the higher is the lipophilicity and the higher is the antiproliferative activity [13,44]. However, no significant differences are observed in terms of antiproliferative activity for the complexes $^{syn}Au_2(^{Mes}L^{OH})(PF_6)_2$ and $^{anti,mix}Au_2(^{Mes}L^{OH})(PF_6)_2$ in both cell lines tested. Exchange of the $(PF_6)^-$ counter-anion in $^{syn}Au_2(^{Mes}L^{OH})(PF_6)_2$ with $Cl^-$ leads to the highly water soluble complex $^{syn}Au_2(^{Mes}L^{OH})(Cl)_2$. It shows no different cytotoxic properties in HeLa cell line. Remarkably, this complex is 7-fold more active in HepG2 cell line (1.85 ± 0.05 μM) than the complex with the $(PF_6)^-$ counter-anion (13.40 ± 3.17 μM), being comparable to auranofin [28].

### 2.4. Mechanistic studies

Considering the mitochondrial enzyme TrxR as well-known target of cationic gold(I) NHC complexes, preliminary mechanistic studies were conducted for both cytotoxic isomers $^{syn}Au_2(^{Mes}L^{OH})(PF_6)_2$ and $^{anti,mix}Au_2(^{Mes}L^{OH})(PF_6)_2$ including auranofin to analyse their inhibition properties particularly focusing on the comparison between both isomers [28,45]. These inhibition studies were performed using a colorimetric method (5,5′-Dithiobis-2-nitrobenzoic acid, DTNB assay) monitoring the reduction of DTNB to TNB (5-thio-2-nitrobenzoic acid) in presence of the enzyme and NADPH [45–47]. The corresponding $IC_{50}$ values were determined by the use of an appropriate range of concentrations and are summarized in Fig. 7.

Both $^{syn}Au_2(^{Mes}L^{OH})(PF_6)_2$ and $^{anti,mix}Au_2(^{Mes}L^{OH})(PF_6)_2$ inhibit mitochondrial TrxR in the nanomolar range ($IC_{50}$ = 145 ± 8 nM and 14 ± 4 nM, respectively). Importantly, $^{syn}Au_2(^{Mes}L^{OH})(PF_6)_2$ displays a similar inhibition ability as auranofin. These results give a first mechanistic insight, showing that this family of complexes could potentially act in the mitochondria targeting TrxR.

The isomeric mixture $^{anti,mix}Au_2(^{Mes}L^{OH})(PF_6)_2$ is a stronger inhibitor of mitochondrial TrxR than $^{syn}Au_2(^{Mes}L^{OH})(PF_6)_2$. These results are in agreement with the higher reactivity against cysteine and with the DFT calculations for the anti-isomer due to less steric and higher accessibility to the gold nuclei. It is still unclear whether the ligands are dissociated and the released gold is entering the selenol-thiol active center or aromatic systems (mesityl) are involved by π-π stacking as shown for another enzyme (aquaporin) by Casini et al. [48].

Further studies are conducted with the isomeric pure $^{syn}Au_2(^{Mes}L^{OH})(PF_6)_2$ since it displays consistent cytotoxicity in HeLa and HepG2 cells. Then, the initially tested cell lines were expanded with two breast cancer cell lines, one prostate, one ovarian and one non-tumoral cell line. The $IC_{50}$ values were obtained under the same conditions mentioned above (Table 2).

The complex $^{syn}Au_2(^{Mes}L^{OH})(PF_6)_2$ displays in general a good cytotoxicity in all the tested cell lines ranging from 1.2 μM in MCF-7

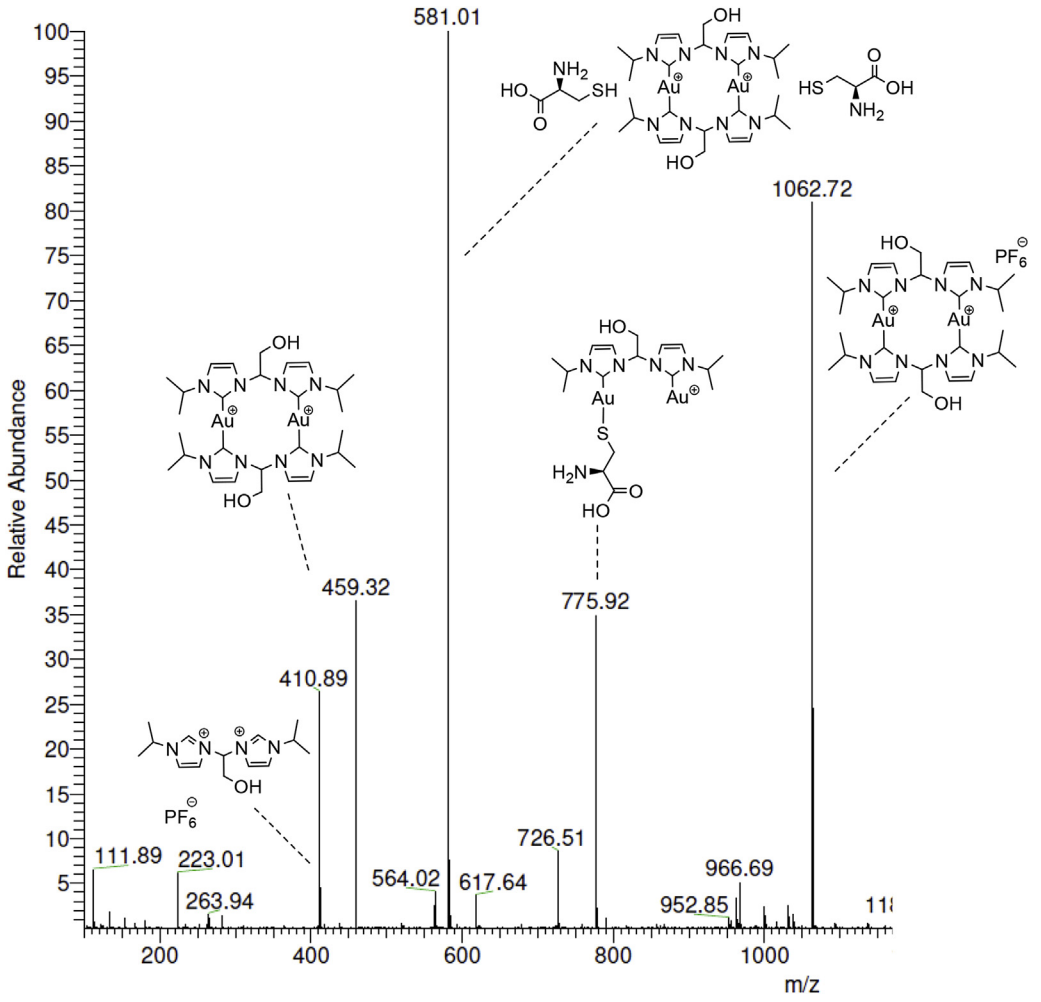


**Fig. 6.** ESI-MS spectrum of reaction mixture of $^{anti}Au_2(^{iPr}L^{OH})(PF_6)_2$ and L-cysteine in DMSO/$H_2O$ (0.35 mL/0.1 mL).

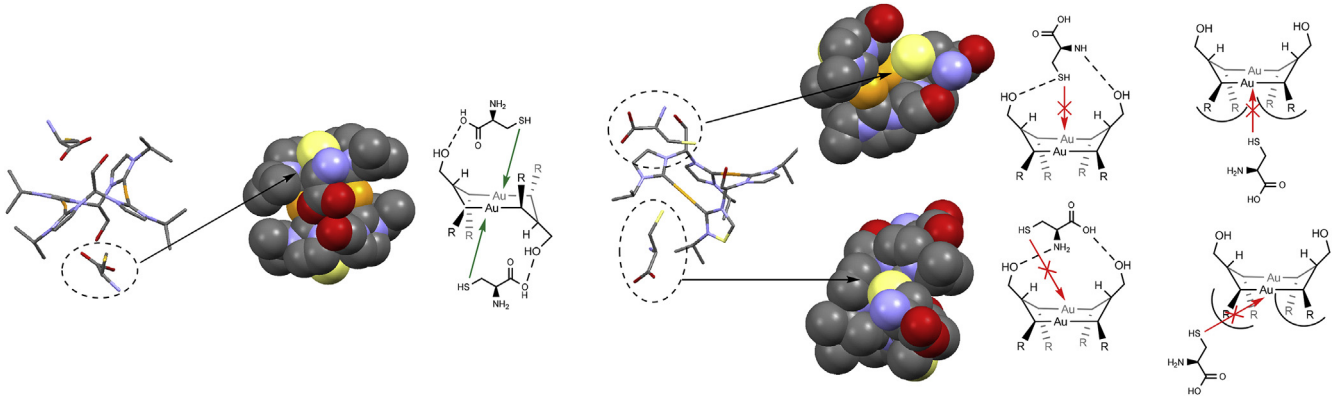

**Scheme 3.** Geometry optimization to analyse the different reactivity of $^{syn}[Au_2(^{OH}L^{iPr})_2](PF_6)_2$ and $^{anti}[Au_2(^{OH}L^{iPr})_2](PF_6)_2$ with two L-cysteine molecules. Density functional: ωB97x-D; basis set: double zeta split valence basis set 6-31G* for non-metals and LANL2DZ, including ECP, for Au. Hydrogen atoms have been omitted for clarity. Colour code: grey: carbon, red: oxygen, blue: nitrogen, orange: gold, yellow: sulphur.

to 18.5 μM in MDA-MB-231, which is better than cisplatin in most cases, particularly in A2780cisR, a cisplatin resistant ovarian cell line. Only a slight difference in the antiproliferative activity between the A2780 cells and the cisplatin resistant ones is observed, showing that the compound overcomes the cisplatin resistance. Moreover, compared to the non-tumoral cell line V79 the complex displays a notable lower activity, indicating a promising selectivity against various types of cancer cells. In particular for the MCF-7 cells, the complex shows a selectivity index (SI) approaching 19, demonstrating superiority over cisplatin and auranofin (SI < 1).

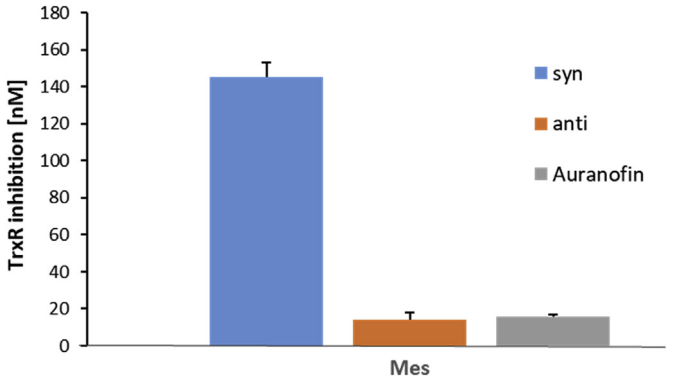


**Fig. 7.** Inhibition study of isolated mitochondrial TrxR by $^{syn}Au_2(^{Mes}L^{OH})(PF_6)_2$ (blue) ($IC_{50}$ = 145 ± 8 nM) $^{anti,mix}Au_2(^{Mes}L^{OH})(PF_6)_2$ (orange) ($IC_{50}$ = 14 ± 4 nM) and **auranofin** (grey) ($IC_{50}$ = 16 ± 1 nM) on isolated mitochondrial TrxR. (For interpretation of the references to colour in this figure legend, the reader is referred to the Web version of this article.)

### 2.5. Cellular gold distribution

The results of the mitochondrial TrxR inhibition assays identified TrxR inhibition as a potential mechanism of action. In the next step, the cellular distribution of gold will be identified by ICP-MS and nuclear microscopy to identify possible targets of the gold compound.

#### 2.5.1. ICP-MS

For a preliminary evaluation of the possible cellular targets of $^{syn}Au_2(^{Mes}L^{OH})(PF_6)_2$, ICP-MS analysis was carried out in cellular fractions of PC3 cells to evaluate the distribution of the complex inside the cells. The cellular distribution of the complex is shown in Fig. 8. The complex is mainly retained in the membranes fraction (70%) that also include the mitochondrial membrane and membrane-bound organelles. Only small amounts were found in the other fractions, although the nucleus represented *ca.* 15%. Results from this study indicate that targets other than the DNA are involved in the mechanism of action. Moreover, through the membrane, the compound could interact with other cellular components including the mitochondria and compromise the cellular viability [49,50].

#### 2.5.2. Nuclear microscopy

To support and substantiate the results obtained by ICP-MS, nuclear microscopy techniques were used to imaging the distribution and depth profile of $^{syn}Au_2(^{Mes}L^{OH})(PF_6)_2$ in whole PC3 cells. The pattern of Au distribution in PC3 cells can be perceived by comparing cell morphology and Au images as displayed in Fig. 9. The mass image show the typical ovoid morphology of the PC3 cell with higher mass density in the centre, likely corresponding to the cell core where most organelles and the nucleus are located. Au was found to be spread through the cell in a dotted pattern (Fig. 9-A). To assess the cellular uptake of the complex, the subsurface layers of the cells were examined by exploring the RBS data and the energy loss of the beam while traversing the cell. A five-layer model with a depth resolution of 294 nm/layer was obtained enabling to reconstruct three-dimensional (3D) images of Au in the cell volume as depicted in Fig. 9-B. The 3D model showed that $^{syn}Au_2(^{Mes}L^{OH})(PF_6)_2$ was internalized by the PC3 cell and that the amount of Au (in terms of number of counts detected, corrected for beam energy loss at different depths) [51] does not differ significantly through cell depth. However, lower Au counts were found at the cell periphery, suggesting that Au is mainly located in the cell core, where organelles and membrane systems are. Thus, the 3D model of Au distribution is consistent with the predominant retention of the $^{syn}Au_2(^{Mes}L^{OH})(PF_6)_2$ complex in the membrane fraction of cells (Fig. 8). The membrane fraction analyzed by ICP-MS includes internal cell membranes, such as mitochondrial membranes, which accounts for at least 40% of total membrane in mammalian cells [52]. Therefore, the $^{syn}Au_2(^{Mes}L^{OH})(PF_6)_2$ complex may interact with mitochondria membrane, where it can inhibit TrxR activity (Fig. 7) to elevate ROS and eventually lead to mitochondria dysfunction.

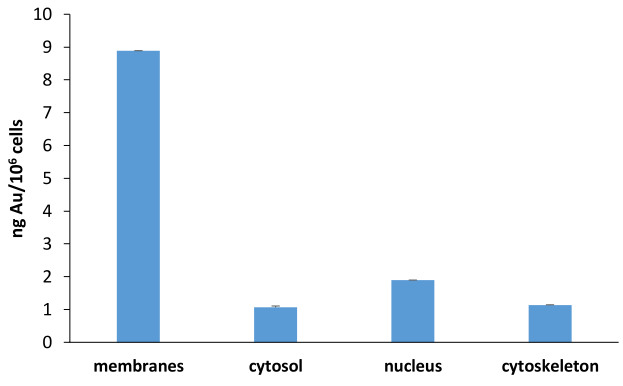


**Fig. 8.** Cellular distribution profile of $^{syn}Au_2(^{Mes}L^{OH})(PF_6)_2$ obtained by ICP-MS.

## 3. Conclusions

Syn- and anti-isomers of previously reported dinuclear Au(I) complexes bearing 2-hydroxyethane-1,1-diyl-bridged bisimidazolylidene ligands have been separated by RP-HPLC and the isolated complexes ($^{anti}Au_2(^{iPr}L^{OH})(PF_6)_2$, $^{syn}Au_2(^{iPr}L^{OH})(PF_6)_2$, $^{anti,mix}Au_2(^{Mes}L^{OH})(PF_6)_2$, $^{syn}Au_2(^{Mes}L^{OH})(PF_6)_2$) were fully characterized.

A first evaluation of the antiproliferative activity of the isolated isomers has shown negligible differences in their cytotoxic behavior in HeLa and HepG2 cell lines. A counter-anion exchange for $^{syn}Au_2(^{Mes}L^{OH})(PF_6)_2$ results in a water-soluble complex $^{syn}Au_2(^{Mes}L^{OH})Cl_2$ with lipophilic mesityl *N*-substituents and leads to antiproliferative activity in HepG2 cell line comparable to auranofin. The stability of all conformational isomers has been examined against L-cysteine and only the anti-isomer shows a single ligand exchange reaction by dissociation of the NHC moiety after 24 h. DFT calculations indicate a higher steric hindrance and more hydrogen bond interaction probability for the syn-isomer. Varying the *N*-substituent to bulkier mesityl groups lead to unreactive conformations. The cytotoxic complexes $^{syn}Au_2(^{Mes}L^{OH})(PF_6)_2$ and $^{anti,mix}Au_2(^{Mes}L^{OH})(PF_6)_2$ inhibit mitochondrial TrxR in the nanomolar range. Thereby, the anti-conformation is a stronger inhibitor, correlating with the observed experimental and *in silico* results, indicating a higher reactivity of the anti-conformation. Expanding the cytotoxic evaluation using several cancer cell lines, representative of common cancer diseases, $^{syn}Au_2(^{Mes}L^{OH})(PF_6)_2$ further exhibits good antiproliferative activity with $IC_{50}$ values ranging from 1.2 (in MCF-7) to 18.5 (in MDA-MB-231) and a selectivity index of 19 in the breast cancer cell line MCF-7 showing the complex's potential importance as a new drug for hormone dependent breast cancer. Especially the high selectivity makes the compound superior to auranofin with exhibits an SI < 1. Further localization studies by ICP-MS and nuclear microscopy reveal that the compound is mainly localized in the membrane. Together with the TrxR affinity assays these results suggest that the mitochondrial membrane is the main target for this type of dinuclear Au(I) *bis*-NHC complexes. Further

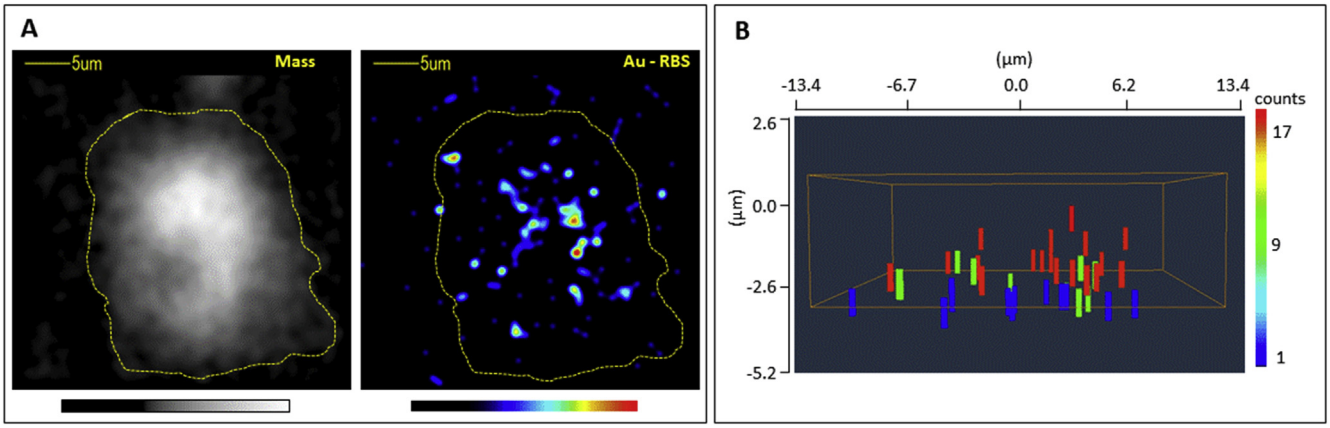


**Fig. 9.** Nuclear microscopy images of mass density (Mass) and Au distribution obtained from the RBS spectrum (Au-RBS) of a PC3 cell incubated with $^{syn}Au_2(^{Mes}L^{OH})(PF_6)_2$ (A). The maps of 37 × 37 μm [2] were obtained by scanning a focused proton beam over the sample surface in 256 × 256 steps. The dotted line indicates the cell contour. (B) 3D representation plot of the model distribution of Au in the cell depicted in (A). Data in layers were compressed to 64 × 64 pixels to better visualize the discrete Au distribution inside the cell. The box represented in the plot set the dimensions for the cell, i) area projection of the cell (approximately 20 μm diameter) and depth (total depth achieved of 1190 nm, for the 5 layers obtained in the model), where zero indicates the surface of the cell; and ii) indicates the point of view and the perspective of the cell in (A). The relative amount of Au in the cell in number of counts is represented by a colour gradient. The mass density and elemental distribution are also represented by a colour gradient with a dynamic scale: high level-white/red; low level-black/deep blue. (For interpretation of the references to colour in this figure legend, the reader is referred to the Web version of this article.)

microscopic studies (e.g. SEM or TEM) would be beneficial to get a deeper inside into the mode of action.

## 4. Experimental

### 4.1. Separation of isomers

**$^{mix}[Au_2(^{iPr}L^{OH})_2](PF_6)_2$**: **$^{anti}[Ag_2(^{iPr}L^{OH})_2](PF_6)_2$** (50 mg, 0.049 mmol, 1.0 eq.)and Au(THT)Cl (32.7 mg, 0.102 mmol, 2.1 eq.) are dissolved in acetonitrile (5 mL) and stirred for 16 h at room temperature under exclusion of light. The resulting precipitate is removed and the solution concentrated. The desired Au(I) complex is obtained as isomer mixture in the second fraction after repeated fractional precipitation using acetonitrile and diethyl ether. The isomer ratio between **$^{anti}[Au_2(^{iPr}L^{OH})_2](PF_6)_2$** and **$^{syn}[Au_2(^{iPr}L^{OH})_2](PF_6)_2$** amounts to 1:0.75. Both isomers are separated by using RP-HPLC technique (C18-column, 5%–50% acetonitrile/water + 0.1% TFA, 15 min, UV-Detection at 215 nm and 280 nm). Acetonitrile is removed *in vacuo*. The resulting oil is extracted with dichloromethane and the organic phases is separately washed with saturated aqueous $NH_4PF_6$ solution (2 × 10 mL) and water (2 × 10 mL). After drying over $MgSO_4$, the organic phase is filtered, concentrated and the desired isolated isomer is crystallized by adding *n*-pentane.

**$^{anti}[Au_2(^{iPr}L^{OH})_2](PF_6)_2$**: RT = 12.65 min; ($^1$H NMR, 400 MHz, $CD_3CN$) $\delta$ (ppm): 7.70 (d [4]$J$ = 2.1 Hz, 4 H, NC***H***CHN), 7.45 (d [4]$J$ = 2.2 Hz, 2 H, NCHC***H***N), 7.36 (t [3]$J$ = 6.5 Hz, 2 H, NC***H***($CH_2OH$)N)), 5.02 (pent [3]$J$ = 6.8 Hz, 2 H, C***H***($CH_3$)$_2$, 4.32 (d [3]$J$ = 6.5 Hz, 4 H, NCH(C***H***$_2$OH)N), 3.90 (t, 2 H, $CH_2O$***H***), 1.50 (dd [3]$J$ = 9.3 Hz [3]$J$ = 6.8 Hz, 24 H, C***H***$_3$); ($^{13}$C NMR, 101 MHz, $CD_3CN$) $\delta$ (ppm): 184.19 (N***C***N), 121.29 (N***C***HCHN), 119.75 (NCH***C***HN), 75.90 (N***C***H($CH_2OH$)N), 62.34 (NCH(***C***H$_2$OH)N), 55.45 (***C***H($CH_3$)$_2$), 23.87 (***C***H$_3$), 23.03 (***C***H$_3$). EA calcd: C 27.83, H 3.67, N 9.27. Found: C 26.60, H 3.50, N 8.7.

**$^{syn}[Au_2(^{iPr}L^{OH})_2](PF_6)_2$**: RT = 14.08 min; ($^1$H NMR, 400 MHz, $CD_3CN$) $\delta$ (ppm) 7.58 (d, $^4J$ = 2.1 Hz, 4 H, NC***H***CHN), 7.44 (t, $^3J$ = 6.1 Hz, 2 H, NC***H***($CH_2OH$)N), 7.41 (d, $^4J$ = 2.1 Hz, 4 H, NCHC***H***N), 4.90 (hept, $^3J$ = 6.8 Hz, 2 H, C***H***($CH_3$)$_2$, 4.38 (t, $^3J$ = 5.1 Hz, 4 H, NCH(C***H***$_2$OH)N), 3.98 (t, $^3J$ = 5.3 Hz, 2 H, $CH_2O$***H***), 1.51 (d, $^3J$ = 6.7 Hz, 12 H, C***H***$_3$), 1.47 (d, $^3J$ = 6.7 Hz, 12 H, C***H***$_3$); ($^{13}$C NMR, 101 MHz, $CD_3CN$) $\delta$ (ppm): 184.31 (N***C***N), 120.76 (N***C***HCHN), 120.06 (NCH***C***HN), 75.03 (N***C***H($CH_2OH$)N), 62.08 (NCH(***C***H$_2$OH)N), 55.48 (***C***H($CH_3$)$_2$), 23.58 (***C***H$_3$), 23.37 (***C***H$_3$). EA calcd: C 27.83, H 3.67, N 9.27. Found: C 27.94, H 3.72, N 9.01.

**$^{mix}[Au_2(^{Mes}L^{OH})_2](PF_6)_2$**: **$^{syn}[Ag_2(^{Mes}L^{OH})_2](PF_6)_2$** (50 mg, 0.037 mmol, 1.0 eq.) and Au(THT)Cl (25.2 mg, 0.079 mmol, 2.1 eq.) are dissolved in acetonitrile (5 mL) and stirred for 16 h at room temperature under exclusion of light. The purification of the isomer mixture is conducted analogue to **$^{mix}[Au_2(^{iPr}L^{OH})_2](PF_6)_2$**. Both isomers are separated by using RP-HPLC technique (C18-column, 30%–70% acetonitrile/water + 0.1%TFA, 25 min, UV-Detection at 215 nm and 280 nm). The same work up technique as in the case of **$^{syn/anti}[Au_2(^{iPr}L^{OH})_2](PF_6)_2$** is applied for both isomers.

**Anti, $^{mix}[Au_2(^{Mes}L^{OH})_2](PF_6)_2$**: RT = 16.28 min; ($^1$H NMR, 400 MHz, $CD_3CN$) $\delta$ (ppm): 7.89 (d, $^4J$ = 2.1 Hz, 4 H, NC***H***CHN), 7.23 (t, 2 H, NC***H***($CH_2OH$)N), 7.21 (d, 4 H, NCHC***H***N), 7.02 (s, 4 H, HMes-aromatic), 6.99 (s, 4 H, HMes-aromatic), 4.33 (d, $^3J$ = 6.4 Hz, 4 H, NCH(C***H***$_2$OH)N), 3.97 (d, 2 H, CH2O***H***), 2.37 (s, 12 H, *p*-C***H***$_3$), 1.88 (s, 12 H, *o*-C***H***$_3$), 1.40 (s, 12 H, *o*-C***H***$_3$), 1.47 (d, $^3J$ = 6.7 Hz, 12 H, C***H***$_3$). ESI MS (*m*/*z*): 611.59 [complex]$^{2+}$.

**$^{syn}[Au_2(^{Mes}L^{OH})_2](PF_6)_2$**: RT = 17.80 min; ($^1$H NMR, 400 MHz, $CD_3CN$): $\delta$ (ppm): 7.79 (d, $^4J$ = 2.1 Hz, 4 H, NC***H***CHN), 7.63 (t, $^3J$ = 5.7 Hz, 2 H, NC***H***($CH_2OH$)N), 7.11 (d, $^4J$ = 2.0 Hz, 4 H, NCHC***H***N), 6.99 (s, 4 H, HMes-aromatic), 6.93 (s, 4 H, HMes-aromatic), 4.55 (t, $^3J$ = 5.4 Hz, 4 H, NCH(C***H***$_2$OH)N), 4.03 (t, $^3J$ = 5.4 Hz, 2 H, $CH_2O$***H***), 2.45 (s, 12 H, *p*-C***H***$_3$), 1.66 (s, 12 H, *o*-C***H***$_3$), 1.37 (s, 12 H, *o*-C***H***$_3$), 1.47 (d, $^3J$ = 6.7 Hz, 12 H, C***H***$_3$). ESI MS (*m*/*z*): 611.61 [complex]$^{2+}$.

### 4.2. Counter-anion exchange

**$^{syn}[Au_2(^{Mes}L^{OH})_2](Cl)_2$**: **$^{syn}[Au_2(^{Mes}L^{OH})_2](PF_6)_2$** (20 mg, 0.013 mmol) are dissolved in methanol (1 mL) and slowly filtered through 2 g of Amberlite IRA 400 Chloride at room temperature in a column. After TLC monitoring and ESI-MS control, methanol was completely evaporated and the oily residue was crystallized by lyophilization of the water solution.

$^1$H NMR (400 MHz, $CD_3CN$, 300 K) $\delta$ (ppm): 8.57 (t, 2 H, $^3J$ = 7.4 Hz, NC***H***($CH_2OH$)N), 7.96 (d, 4 H, $^4J$ = 2.1 Hz, NC***H***CHN), 7.08 (d, 4 H, $^4J$ = 2.1 Hz, NCHC***H***N), 6.95–6.89 (m, 8 H, HMes-aromatic), 4.54 (d, 4 H, $^3J$ = 7.4 Hz, NCH(C***H***$_2$OH)N), 2.45 (s, 12 H, *p*-C***H***$_3$), 1.68 (s, 12 H, *o*-C***H***$_3$), 1.38 (s, 12 H, *o*-C***H***$_3$). ($^{13}$C NMR, 101 MHz, Cryo, $CD_3CN$) $\delta$ (ppm): 186.20 (s, 4C, N***C***N), 140.40 (*o*-$CH_3$C***C***N), 135.38 (*p*-

$CH_3$***C***), 135.33 (*o*-$CH_3$***C***CN), 135.24 (*o*-$CH_3$***C***CN), 130.21 (***C***$H_{Mes}$), 130.06 (***C***$H_{Mes}$), 125.56 (N***C***HCHN), 119.73 (NCH***C***HN), 61.21 (NCH(***C***$H_2$OH)N), 21.31 (***C***$H_3$), 17.37 (***C***$H_3$). ESI MS (m/Z): 611.71 $[complex]^{2+}$, 1256.93 [complex + Chlorid]$^+$. EA calcd: C 48.27, H 4.67, N 8.66. Found: C 45.37, H 4.72, N 7.91. $^1$H NMR (400 MHz, $D_2O$, 300 K) $\delta$ (ppm): 7.87 (d, 4 H, $^4J$ = 2.1 Hz, NC***H***CHN), 7.82–7.76 (m, 2 H, NC***H***($CH_2$OH)N), 7.20 (d, 4 H, $^4J$ = 2.1 Hz, NC***H***CHN), 7.05–7.03 (m, 4 H, HMes-aromatic), 6.98 (s, 4 H, HMes-aromatic), 4.69 (d, 4 H, $^3J$ = 6.6 Hz, NCH(C***H***$_2$OH)N), 2.46 (s, 12 H, *p*-C***H***$_3$), 1.69 (s, 12 H, *o*-C***H***$_3$), 1.40 (s, 12 H, *o*-C***H***$_3$).

### 4.3. Reactivity studies in the presence of L-cysteine

NMR-scale experiments were conducted for the reactivity studies of $^{anti}$**[Au$_2$($^{iPr}$L$^{OH}$)$_2$](PF$_6$)$_2$**, $^{syn}$**[Au$_2$($^{iPr}$L$^{OH}$)$_2$](PF$_6$)$_2$**, $^{syn}$**[Au$_2$($^{Mes}$L$^{OH}$)$_2$](PF$_6$)$_2$**, $^{anti,\ mix}$**[Au$_2$($^{Mes}$L$^{OH}$)$_2$](PF$_6$)$_2$** and **Au-ref** with L-cysteine. Therefore, Au(I) complex (10 mg, 1.0 eq.) and L-cysteine (4.5 eq.) were dissolved in DMSO-$d_6$ (0.35 mL) and $D_2O$ (0.1 mL) and heated to 37 °C for 24 h in a NMR tube. The reaction was monitored by measuring a proton NMR after 0 h, 2 h, 4 h, 6 h, 8 h and 24 h. After 24 h, the reaction mixture was finally diluted in acetonitrile and injected in ESI-MS.

### 4.4. Cell viability/antiproliferative studies (MTT-Assay)

Cells (1–8x10$^4$ cells per well) in RPMI medium (Gibco, Invitrogen) supplemented with 10% FBS were seeded in 96 well plates for 24 h to reach 30–40% confluence. Then, the medium was removed and the tested complexes at serial concentrations in medium (200 μL) were added to the cells. The percentage of DMSO did not exceed 1% and, at this concentration, was without cytotoxic effect. After an incubation time of 48 h, 20 μL of MTT (thiazolyl blue tetrazolium bromide) (20 μL, 5 mg/mL in Millipore water, Sigma Aldrich) were added to the cells and incubated for further 3 h. After removal of the medium, the resulting formazan crystals were dissolved in DMSO (150 μL). The optical density was measured at 570 nm and background subtracted at 630 nm using a Tecan Infinite® M200 Pro. The $IC_{50}$ values were calculated from dose-response curves obtained using GraphPad Prism software (*vs* 5.0).

### 4.5. Thioredoxin reductase (TrxR) inhibition studies

Inhibition studies on isolated TrxR (rat liver) were performed using a commercially available Thioredoxin Reductase Kit (Sigma Aldrich) *via* the DTNB (5,5′-Dithiobis-2-nitrobenzoic acid) assay. The assay is based on the reduction of DTNB by NADPH to 5-thio-2-nitrobenzoic acid (TNB). The experiments were conducted in a 96 well plate including a blank, a positive control, a control inhibitor and the tested complexes in varied concentrations in a total volume of 200 μL. The enzyme, DTNB and inhibitor solutions as well as the assay buffers were prepared according to the Kit instructions. After slightly shaking for 2 h at room temperature, the formation of TNB (5-thio-2-nitrobenzoic acid) was monitored at 412 nm using a Tecan Infinite® M200 Pro multi-plate reader.

### 4.6. Cellular gold distribution by ICP-MS

The cellular gold content was analyzed by a Thermo X-Series Quadrupole ICP-MS. PC3 cells (approx. 10$^6$ cells/5 mL medium) were exposed to the compound at 50 μM for 1.5 h at 37 °C in an incubator with 5% $CO_2$ and humidified atmosphere, then washed with ice-cold PBS and centrifuged to obtain a cellular pellet. The cytosol, membranes/particulate, cytoskeletal and nuclear fractions were isolated using a FractionPREP™, cell fractionation system (BioVision, USA) and performed according to the manufacturer's recommendations. The gold content in the different fractions was measured after digestion of the samples in a closed pressurized microwave digestion unit (Mars5, CEM) with medium pressure HP500 vessels and then diluted in ultrapure water to obtain 2.0% (v/v) nitric acid. The instrument was tuned using a multi element ICP-MS 71 C standard solution (Inorganic Venture). Indium ($^{115}$In) at 10 μM was used as internal standard.

### 4.7. Cellular gold distribution and depth profile by nuclear microscopy

PC3 cells were seeded on 100 nm thick silicon nitride ($Si_3N_4$) membranes (Silson Ltd., UK) and incubated with the complex at 50 μM for 1.5 h. The culture medium was carefully removed and the monolayer of cells adherent onto the $Si_3N_4$ membrane was washed with cold PBS, cryofixed and allowed to dry in a cryostat at −25 °C overnight. The Au distribution in individual PC3 cells was assessed by nuclear microscopy. The nuclear microscopy experiments were performed at the nuclear microprobe facility of Instituto Superior Técnico using a proton beam of 2 MeV focused to micrometer dimensions [53]. By scanning the beam over a region of interest of the sample two-dimensional (2D) images of morphological details, mass density and elemental distribution can be delivered together with depth profiling information extracted from the calculated beam energy loss with Rutherford backscattering spectrometry (RBS) which enables to reconstruct three-dimensional (3D) images of Au in the whole cells using the software MORIA.[52, 53] Acquisition of data was performed using OMDAQ 2007 (Oxford Microbeams Ltd, UK).

## Declaration of competing interest

The authors declare that they have no known competing financial interests or personal relationships that could have appeared to influence the work reported in this paper.

## Acknowledgements

BD, CHGJ, JO, PJF and EME acknowledge the TUM Graduate School for financial support. JDGC and FM gratefully acknowledge the Fundação para a Ciência e a Tecnologia, Portugal, for financial support through projects UID/Multi/04349/2019 and PTDC/QUI-NUC/30147/2017. TP acknowledges the support of the Fundação para a Ciência e Tecnologia, Portugal, through the projects UID/BIO/04565/2020 and Programa Operacional Regional de Lisboa 2020 (Project N. 007317). BD thanks for cooperation and technical support with the group of Buchner (Cell culturing devices) and of Sieber (Multi-reader for MTT- and DTNB-assays) as well as Fiona Kiefer, Franziska Schuderer and Nicholas Lim for experimental support. Eugénio Soares from LCA- Aveiro University, Portugal is acknowledged for the analyses of ICP-MS.

## Appendix A. Supplementary data

Supplementary data to this article can be found online at https://doi.org/10.1016/j.ejmech.2020.112576.

## References

[1] W.K. Liu, R. Gust, Coord. Chem. Rev. 329 (2016) 191–213.
[2] M. Porchia, M. Pellei, M. Marinelli, F. Tisato, F. Del Bello, C. Santini, Eur. J. Med. Chem. 146 (2018) 709–746.
[3] B. Dominelli, J.D.G. Correia, F.E. Kühn, J. Organomet. Chem. 866 (2018) 153–164.
[4] S.Y. Hussaini, R.A. Haque, M.R. Razali, J. Organomet. Chem. 882 (2019) 96–111.
[5] M. Mora, M.C. Gimeno, R. Visbal, Chem. Soc. Rev. 48 (2019) 447–462.

[6] I. Ott, Coord. Chem. Rev. 253 (2009) 1670–1681.
[7] L. Kelland, Nat. Rev. Canc. 7 (2007) 573–584.
[8] V. Brabec, O. Hrabina, J. Kasparkova, Coord. Chem. Rev. 351 (2017) 2–31.
[9] B.W. Harper, A.M. Krause-Heuer, M.P. Grant, M. Manohar, K.B. Garbutcheon-Singh, J.R. Aldrich-Wright, Chem. Eur J. 16 (2010) 7064–7077.
[10] C.P. Tan, Y.Y. Lu, L.N. Ji, Z.W. Mao, Metall 6 (2014) 978–995.
[11] X. Chen, X. Shi, C. Zhao, X. Li, X. Lan, S. Liu, H. Huang, N. Liu, S. Liao, D. Zang, W. Song, Q. Liu, B.Z. Carter, P.Q. Dou, X. Wang, J. Liu, Oncotarget 5 (2014) 9118–9132.
[12] M.N. Hopkinson, C. Richter, M. Schedler, F. Glorius, Nature 510 (2014) 485–496.
[13] P.J. Barnard, M.V. Baker, S.J. Berners-Price, D.A. Day, J. Inorg. Biochem. 98 (2004) 1642–1647.
[14] E.O. Natalia, G. Federica, I.A.M. de Graaf, M. Lorella, d.J.M. H, G.G.M. M, G. Chiara, C. Angela, ChemMedChem 12 (2017) 1429–1435.
[15] T.T. Zou, C.N. Lok, P.K. Wan, Z.F. Zhang, S.K. Fung, C.M. Che, Curr. Opin. Chem. Biol. 43 (2018) 30–36.
[16] M.-M. Gan, J.-Q. Liu, L. Zhang, Y.-Y. Wang, F.E. Hahn, Y.-F. Han, Chem. Rev. 118 (2018) 9587–9641.
[17] S.J. Berners-Price, A. Filipovska, Metall 3 (2011) 863–873.
[18] J.S. Modica-Napolitano, J.R. Aprille, Adv. Drug Deliv. Rev. 49 (2001) 63–70.
[19] L.B. Chen, Annu. Rev. Cell Biol. 4 (1988) 155–181.
[20] S. Gromer, L.D. Arscott, C.H. Williams, R.H. Schirmer, K. Becker, J. Biol. Chem. 273 (1998) 20096–20101.
[21] S. Gromer, S. Urig, K. Becker, Med. Res. Rev. 24 (2004) 40–89.
[22] A. Bindoli, M.P. Rigobello, G. Scutari, C. Gabbiani, A. Casini, L. Messori, Coord. Chem. Rev. 253 (2009) 1692–1707.
[23] V. Gandin, A.P. Fernandes, M.P. Rigobello, B. Dani, F. Sorrentino, F. Tisato, M. Bjornstedt, A. Bindoli, A. Sturaro, R. Rella, C. Marzano, Biochem. Pharmacol. 79 (2010) 90–101.
[24] B. Bertrand, A. de Almeida, E.P.M. van der Burgt, M. Picquet, A. Citta, A. Folda, M.P. Rigobello, P. Le Gendre, E. Bodio, A. Casini, Eur. J. Inorg. Chem. 2014 (2014) 4532–4536.
[25] E.R.T. Tiekink, Crit. Rev. Oncol. Hematol. 42 (2002) 225–248.
[26] T. Zou, C.T. Lum, C.-N. Lok, W.-P. To, K.-H. Low, C.-M. Che, Angew. Chem. Int. Ed. 53 (2014) 5810–5814.
[27] R. Zhong, A. Pöthig, D.C. Mayer, C. Jandl, P.J. Altmann, W.A. Herrmann, F.E. Kühn, Organometallics 34 (2015) 2573–2579.
[28] J. Rieb, B. Dominelli, D. Mayer, C. Jandl, J. Drechsel, W. Heydenreuter, S.A. Sieber, F.E. Kühn, Dalton Trans. 46 (2017) 2722–2735.
[29] B. Dominelli, G.M. Roberts, C. Jandl, P.J. Fischer, R.M. Reich, A. Pöthig, J.D.G. Correia, F.E. Kühn, Dalton Trans. 48 (2019) 14036–14043.
[30] R. Zhong, A. Pöthig, S. Haslinger, B. Hofmann, G. Raudaschl-Sieber, E. Herdtweck, W.A. Herrmann, F.E. Kühn, ChemPlusChem 79 (2014) 1294–1303.
[31] Y.-F. Han, G.-X. Jin, C.G. Daniliuc, F.E. Hahn, Angew. Chem. Int. Ed. 54 (2015) 4958–4962.
[32] L.E. Wedlock, P.J. Barnard, A. Filipovska, B.W. Skelton, S.J. Berners-Price, M.V. Baker, Dalton Trans. 45 (2016) 12221–12236.
[33] Z. Chen, Z. Li, L. Yang, J. Liang, J. Yin, G.-A. Yu, S.H. Liu, Dyes Pigments 121 (2015) 170–177.
[34] R.M. Almotawa, G. Aljomaih, D.V. Trujillo, V.N. Nesterov, M.A. Rawashdeh-Omary, Inorg. Chem. 57 (2018) 9962–9976.
[35] A. Maspero, I. Kani, A.A. Mohamed, M.A. Omary, R.J. Staples, J.P. Fackler, Inorg. Chem. 42 (2003) 5311–5319.
[36] M. Preisenberger, P. Pyykkö, A. Schier, H. Schmidbaur, Inorg. Chem. 38 (1999) 5870–5875.
[37] W.E. van Zyl, J.M. López-de-Luzuriaga, A.A. Mohamed, R.J. Staples, J.P. Fackler, Inorg. Chem. 41 (2002) 4579–4589.
[38] J.B. Foley, A. Herring, B. Li, E.V. Dikarev, Inorg. Chim. Acta. 392 (2012) 300–310.
[39] M.A. Rawashdeh-Omary, M.A. Omary, J.P. Fackler, Inorg. Chim. Acta. 334 (2002) 376–384.
[40] A. Biffis, M. Cipani, C. Tubaro, M. Basato, M. Costante, E. Bressan, A. Venzo, C. Graiff, New J. Chem. 37 (2013) 4176–4184.
[41] R. Gericke, M.A. Bennet, S.H. Priver, S.K. Bhargav, Organometallics 36 (2017) 3178–3188.
[42] A.K. Hijazi, N. Radhakrishnan, K.R. Jain, E. Herdtweck, O. Nuyken, H.-M. Walter, P. Hanefeld, B. Voit, F.E. Kühn, Angew. Chem. Int. Ed. 46 (2007) 7290–7292.
[43] P.J. Altmann, A. Pöthig, J. Am. Chem. Soc. 138 (2016) 13171–13174.
[44] M.V. Baker, P.J. Barnard, S.J. Berners-Price, S.K. Brayshaw, J.L. Hickey, B.W. Skelton, A.H. White, Dalton Trans. 30 (2006) 3708–3715.
[45] V. Rodríguez-Fanjul, E. López-Torres, M.A. Mendiola, A.M. Pizarro, Eur. J. Med. Chem. 148 (2018) 372–383.
[46] S. Jürgens, V. Scalcon, N. Estrada-Ortiz, A. Folda, F. Tonolo, C. Jandl, D.L. Browne, M.P. Rigobello, F.E. Kühn, A. Casini, Biorg. Med. Chem. 25 (2017) 5452–5460.
[47] R. Rubbiani, I. Kitanovic, H. Alborzinia, S. Can, A. Kitanovic, L.A. Onambele, M. Stefanopoulou, Y. Geldmacher, W.S. Sheldrick, G. Wolber, A. Prokop, S. Wolfl, I. Ott, J. Med. Chem. 53 (2010) 8608–8618.
[48] M.N. Wenzel, A.F. Mósca, V. Graziani, B. Aikman, S.R. Thomas, A. de Almeida, J.A. Platts, N. Re, C. Coletti, A. Marrone, G. Soveral, A. Casini, Inorg. Chem. 58 (2019) 2140–2148.
[49] L. Côrte-Real, A.P. Matos, I. Alho, T.S. Morais, A.I. Tomaz, M.H. Garcia, I. Santos, M.P. Bicho, F. Marques, Microsc. Microanal. 19 (2013) 1122–1130.
[50] L. Côrte-Real, F. Mendes, J. Coimbra, T.S. Morais, A.I. Tomaz, A. Valente, M.H. Garcia, I. Santos, M. Bicho, F. Marques, J. Biol. Inorg. Chem. 19 (2014) 853–867.
[51] M.S. Vasco, L.C. Alves, V. Corregidor, D. Correia, C.P. Godinho, I. Sá-Correia, A. Bettiol, F. Watt, T. Pinheiro, J. Microsc. 267 (2017) 227–236.
[52] R.a. Milo, Cell Biology by the Numbers, Garland Science, New York, NY, 2016.
[53] A. Veríssimo, L.C. Alves, P. Filipe, J.N. Silva, R. Silva, M. Dolores Ynsa, E. Gontier, P. Moretto, J. Pallon, T. Pinheiro, Microsc. Res. Tech. 70 (2007) 302–309.